International Journal of Heat and Mass Transfer 196 (2022) 123304

Contents lists available at ScienceDirect

International Journal of Heat and Mass Transfer

journal homepage: www.elsevier.com/locate/hmt

A new analytical model for the conduction shape factor of annulus sectors

Callum Chhokar, G. Bamorovat Abadi, Majid Bahrami*

Laboratory for Alternative Energy Conversion (LAEC), School of Mechatronic Systems Engineering, Simon Fraser University, Burnaby, BC V3T 0A3, Canada

ARTICLE INFO

Article history:
Received 21 April 2022
Revised 9 July 2022
Accepted 25 July 2022

Keywords:
Microelectronics cooling
Thermal management
Conduction
Thermal resistance
Hollow cylinder

ABSTRACT

Heat transfer devices, such as heat pipes, vapor chambers, thermosiphons, microchannel heat sinks, and Peltier cooling plates, rely on two-dimensional steady heat conduction to thermally manage telecommunications, aerospace, and microelectronics heat-generating components. The conduction shape factor can evaluate these devices' two-dimensional steady heat conduction. The geometry of the device's annulus and its mechanical attachment to the heat-generating component can vary. Given the prominence of single-sided heating and cooling, the two-dimensional heat conduction is commonly through an annulus sector. For the first time, an analytical model is developed to predict the conduction shape factor of annulus sectors. The present model is an extension of the previously developed equivalent concentric circular annulus model and applies the equivalent concentric circular annulus sector. The model is validated with results from finite element modeling for parametric boundary geometries, capturing most of the data across a variety of sectors within a relative difference of 10%. The present model provides a simple, closed-form analytical solution for the shape factor of an annulus sector formed between concentric arbitrarily shaped isothermal boundaries. More importantly, it provides a unified platform for designing and optimizing novel heat transfer devices.

1. Introduction

Heat transfer devices, such as heat pipes, vapor chambers, thermosiphons, microchannel heat sinks, and Peltier cooling plates rely on two-dimensional steady heat conduction in an annulus or annulus sector to thermally manage products with applications in telecommunications, aerospace, and microelectronics industries. Fig. 1 illustrates a few examples of such devices. Heat pipes, pulsating heat pipes, and microchannel heat sinks require low conduction thermal resistance to effectively transfer heat to and from a working fluid. These devices are of varying geometry, owing to their shape-based research and development. Given their application, they can be subjected to heating and cooling of a varying proportion of their outer wall(s).

For a two-dimensional region with an enclosed material that has constant thermal conductivity, the thermal resistance between the outer and inner boundaries is inversely proportional to the conduction shape factor per unit depth [1]:

$$S = \frac{1}{kR} = \frac{\dot{Q}}{k\Delta T} = \frac{\dot{Q}}{k|T_o - T_i|} \tag{1}$$

where S, k, R, $\dot{Q}$, T_o and T_i are the shape factor per unit depth, thermal conductivity, thermal resistance, heat power, and outer and inner boundary temperature, respectively (see Fig. 2).

The shape factor per unit depth of a concentric circular annulus has an exact analytical solution as follows [2]:

$$S = \frac{2\pi}{\ln(d_o/d_i)} \tag{2}$$

where, as shown in Fig. 2, d_o and d_i are the outer and inner diameter, respectively.

Using Eq. (2), Teertstra et al. [8] developed a shape factor model for arbitrary concentric shapes known as the *two-rule* method. The two-rule method uses an equivalent concentric circular annulus. The inner and outer diameters of the equivalent concentric circular annulus are calculated by preserving the inner perimeter and the enclosed area. The shape factor per unit depth can then be approximated as follows:

$$P_i = \pi d_i \rightarrow d_i = P_i/\pi$$

$$A = \frac{\pi}{4}\left(d_o^2 - d_i^2\right) \rightarrow d_o = \sqrt{\frac{4}{\pi}A + d_i^2}$$

$$S = \frac{2\pi}{\ln\left[\sqrt{4\pi\left(A/P_i^2\right) + 1}\right]} \tag{3}$$

* Corresponding author.
E-mail address: mbahrami@sfu.ca (M. Bahrami).

https://doi.org/10.1016/j.ijheatmasstransfer.2022.123304
0017-9310/

Nomenclature

a	hyperellipse characteristic dimension [m]
m	polygon number of sides
ℓ	nondimensional characteristic length scale, $\equiv \sqrt{A}/s_i$
A	area [m^2]
ℓ^*	modified nondimensional characteristic length scale
d	diameter [m]
r	radial coordinate [m]
P	perimeter [m]
$\dot{Q}$	heat power [W]
T	temperature [K]
R	thermal resistance [KW^{-1}]
k	thermal conductivity [$Wm^{-1}K^{-1}$]
L	length (or depth) [m]
S	shape factor per unit depth
n	hyperellipse exponent parameter
s	sector boundary length [m]

Greek symbols

ϵ	aspect ratio
δ	wall thickness [m]
α	equivalent circular annulus sector angle [rad]
ζ	blending parameter
θ	angular coordinate [rad]
ρ	circumradius [m]
Δ	apothem [m], $\equiv \rho \cos(\pi/m)$
ϕ	sector angle [rad]
η	unit normal vector

Subscripts

i	inner
o	outer
min	minimum
max	maximum
HT	heat transfer

where A and P_i are the enclosed area and inner perimeter, respectively. The two-rule method shape factor can be written in terms of a nondimensional characteristic length scale, ℓ, as follows:

$$\ell = \sqrt{A}/P_i$$
$$S = \frac{2\pi}{\ln\left[\sqrt{4\pi\ell^2+1}\right]} \tag{4}$$

Teertstra *et al.* [9] further developed the method for nonuniform wall thickness and thermal æshort-circuitingg using an asymptotic approach:

$$\ell^* = \left[\ell^\zeta - \left(\lim_{\delta_{\min}\to 0}\ell\right)^\zeta\right]^{1/\zeta}$$
$$S = \frac{2\pi}{\ln\left[\sqrt{4\pi(\ell^*)^2+1}\right]} \tag{5}$$

where $\delta_{\min}$ is the minimum wall thickness, ζ is a blending parameter whose value was selected to provide a good overall agreement with the available data, and ℓ^* is the modified nondimensional characteristic length scale. Teertstra et al. reported that $\zeta = 3$ was appropriate.

Other annulus shape factor models exist. Simeza and Yovanovich [1] used the parallel flux-tube heat flow model [10] for the polygonal cylinder with a concentric circular hole to develop the following model for the shape factor per unit depth:

$$\psi^2 = \ln\left(\frac{2\Delta}{d_i}\right)$$
$$S = 2m\left\{\frac{1}{\psi\sqrt{\psi^2+0.5}}\tan^{-1}\left[\frac{\sqrt{\psi^2+0.5}}{\psi}\tan\left(\frac{\pi}{m}\right)\right]\right\} \tag{6}$$

where Δ is the apothem, the distance from the center to the midpoint of one of the sides, and m is the number of polygon sides.

Hassani and Hollands [11] used a similar approach and developed a model for the shape factor per unit depth upper bound for identical boundary shapes (i.e., uniform wall thickness), such as concentric squares, triangles, rhombic cylinders, and rectangles:

$$S_{\max} = \frac{2\pi}{\ln[1+(2\pi\delta/P_i)]} \tag{7}$$

where δ and P_i are the wall thickness and inner perimeter, respectively.

Numerical methods have also been developed. Given the definition of thermal resistance and shape factor, shown in Eq. (1), Hirbodi and Jafarpur [12] used the heat transfer area to length ratio to approximate the shape factor of any arrangement of m-sided polygons. Integral and weighted averaging methods were used to estimate the heat transfer length, L_{HT}, and area, A_{HT}.

$$SL = \frac{1}{kR} = \frac{1}{k(L_{\mathrm{HT}}/kA_{\mathrm{HT}})} = \frac{A_{\mathrm{HT}}}{L_{\mathrm{HT}}} \tag{8}$$

Although there are several conduction shape factor models for the annulus formed between concentric inner and outer isothermal boundaries, there is no analytical model in the literature for the annulus sector. This study fills this gap by developing a new and accurate closed-form analytical solution to predict the shape factor for the annulus sector formed between concentric arbitrarily shaped boundaries.

This study uses the following approach:

1. The analytical model is developed (Model development).
2. The analytical model is extensively validated with finite element modeling results for all-encompassing, parametrically-defined geometries (Results and discussion).
3. Conclusions, including limitations, are drawn from the present model's agreement with the finite element modeling results (Results and discussion, Summary and conclusions).

2. Model development

The present model extends Teertstra et al.' s two-rule method [8], shown in Eq. (3), to consider an arbitrarily-shaped concentric annulus sector subject to partial inner and outer isothermal boundary conditions. Fig. 3 shows the equivalent concentric circular annulus sector for a concentric hexagonal annulus sector. The outer isothermal boundary condition spans a larger length than the inner isothermal boundary condition (i.e., $s_o > s_i$). The remaining outer perimeter is insulated. The inner perimeter may be partially or entirely isothermal (i.e., $s_i \le P_i$); however, the model neglects temperature gradients that are normal to the sector's angular extents (i.e., the model considers a null temperature gradient in the θ-direction at the sector's θ extents). Neglecting these gradients underestimates the shape factor. In doing so, the model overestimates thermal resistance. Consistent with the nature of the two-rule method, isotherms are assumed to be equivalently radial, or parallel to the inner and outer boundaries (s_i and s_o). Thus, thick, small-angle sectors, which may be better modeled with a thermal spreading resistance, are not considered. Extending the two-rule

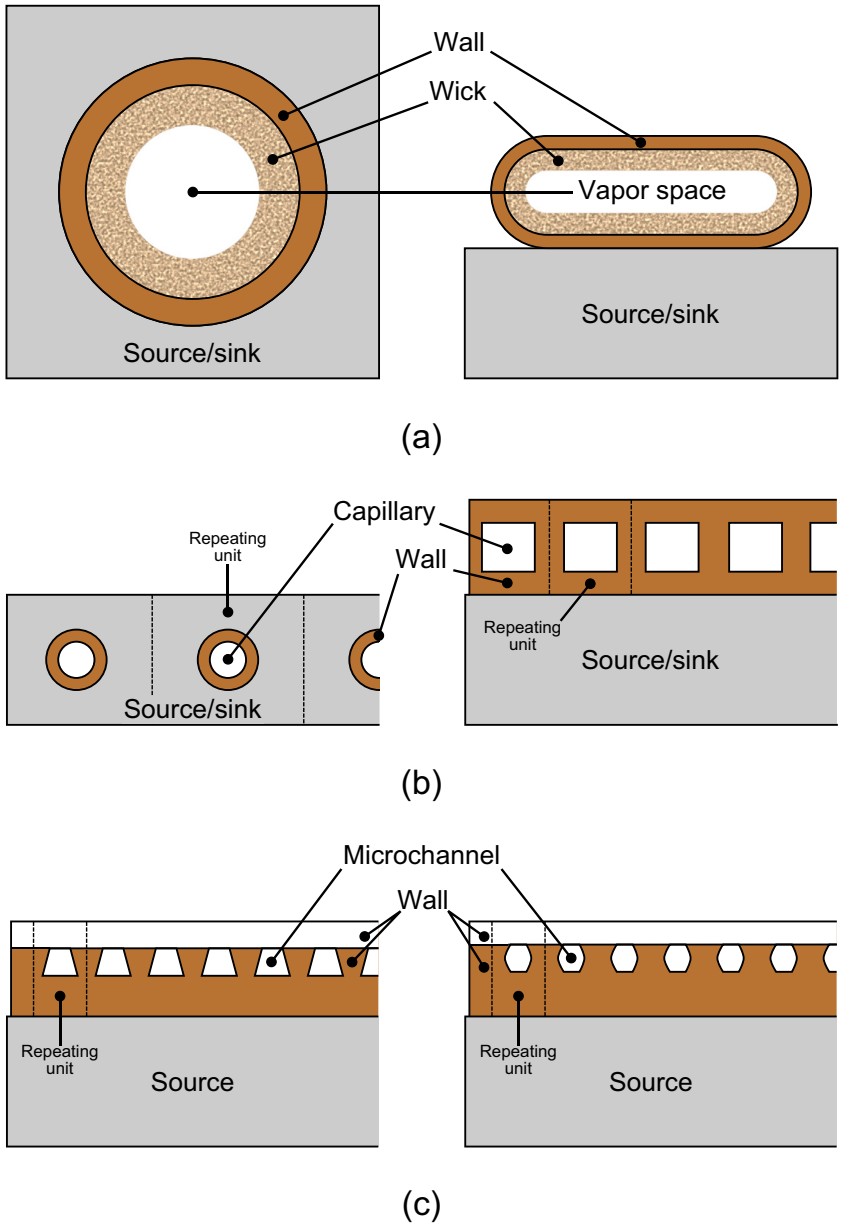

Fig. 1. A schematic representation of the cross-sections of a) round and flat heat pipes (e.g., [3,4]), b) tubular and flat-plate pulsating heat pipes (e.g., [5,6]), and c) microchannel heat sinks (e.g., [7]). The repeating unit can be considered an annulus for the latter two devices. These devices have been manufactured with varying cross-sectional geometry, an active area of their research and development, and used in various heating and cooling configurations.

method, the shape factor of the sector is as follows:

$$S = \frac{\alpha}{\ln\left[\sqrt{2\alpha\left(A/s_i^2\right)+1}\right]} \tag{9}$$

where A and s_i are the sector's area and inner boundary length, respectively, and α is the angle of the equivalent circular annulus sector, which is an estimated quantity, and not the angle of the sector, ϕ. Similar to the analysis for the entire annulus in Eq. (4), the shape factor can be written in terms of a nondimensional characteristic length scale as follows:

$$\ell = \sqrt{A}/s_i$$

$$S = \frac{\alpha}{\ln\left[\sqrt{2\alpha\ell^2+1}\right]} \tag{10}$$

where ℓ and α are the nondimensional characteristic length scale and equivalent sector's angle, respectively. A third rule is proposed in this study to approximate the equivalent sector's angle. This rule preserves the outer boundary length of the sector. This rule is combined with the two-rule method, Eq. (3):

$$s_o = \frac{\alpha}{2} d_o$$

$$\alpha = \frac{1}{2}\left(\frac{s_o^2}{A} - \frac{s_i^2}{A}\right) = \frac{1}{2\ell^2}\left[\left(\frac{s_o}{s_i}\right)^2 - 1\right] \le 2\pi \tag{11}$$

where A, s_o, and s_i are the sector's area, and outer and inner boundary length, respectively. The equivalent sector's angle is limited to that of an entire annulus (i.e., $\alpha \le 2\pi$).

Eqs. (10) and (11) are used to calculate the shape factor of the sector. For an annulus with uniform wall thickness, the shape factor can be simplified:

$$S = \frac{\alpha}{\ln\left(s_o/s_i\right)} = \frac{\left(s_o/s_i\right)^2 - 1}{2\ell^2 \ln\left(s_o/s_i\right)}, \quad \alpha \le 2\pi \tag{12}$$

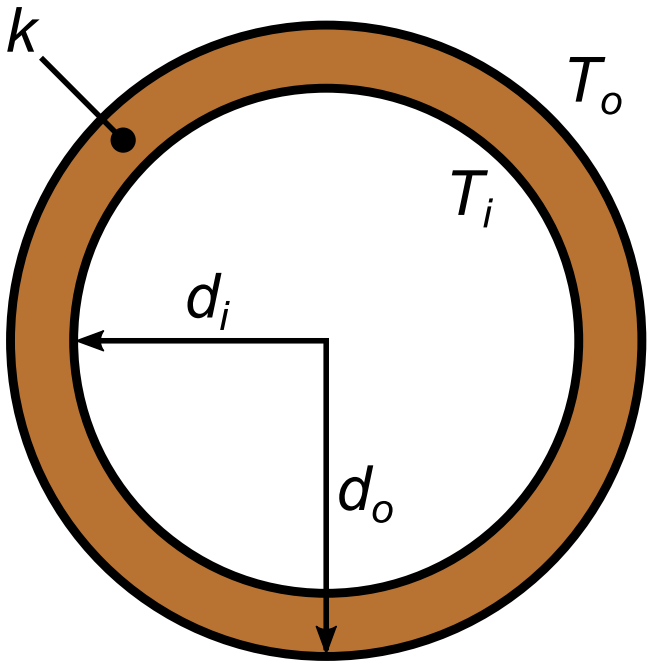

Fig. 2. Concentric circular annulus.

where ℓ is the nondimensional characteristic length scale, defined in Eq. (10), and s_o/s_i is the sector's outer to inner boundary length ratio. For equivalent sector angles above 2π, the sector is likened to an entire annulus and the two-rule method is used, Eq. (4).

As mentioned and shown in Eq. (5), Teertstra et al. [9] further developed the two-rule method for dissimilar boundaries, where the annulus may have a highly nonuniform wall thickness. As shown in Fig. 4, the same asymptotic blending approach is used for the present model, where the sector's nondimensional characteristic length scale is modified, $\ell \rightarrow \ell^*$, before using Eq. (10) to calculate the sector shape factor:

$$\ell^* = \left[\ell^\zeta - \left(\lim_{\delta_{\min}\rightarrow 0} \ell\right)^\zeta\right]^{1/\zeta}$$
$$\alpha = \frac{1}{2\ell^2}\left[\left(\frac{s_o}{s_i}\right)^2 - 1\right] \leq 2\pi$$
$$S = \frac{\alpha}{\ln\left[\sqrt{2\alpha(\ell^*)^2 + 1}\right]} \tag{13}$$

where $\delta_{\min}$ is the minimum wall thickness, ζ is a chosen blending parameter chosen as three following Teertstra et al. [9], and ℓ^* is the sector's modified nondimensional characteristic length scale. As previously mentioned, a blending parameter of three provided a good overall agreement with available entire annulus conduction shape factor data as reported by Teertstra et al. [9]. The blending parameter is a fitted parameter that can significantly change the sector shape factor calculated by the present model (Eq. (13)) and the entire annulus shape factor model of Teertstra et al. [9]. As will be shown in the results and discussion of this study, a value of three provided not only good agreement with experimental data for Teertstra et al. [9] but also good agreement with finite element modeling results for the wide variety of investigated annulus sec-

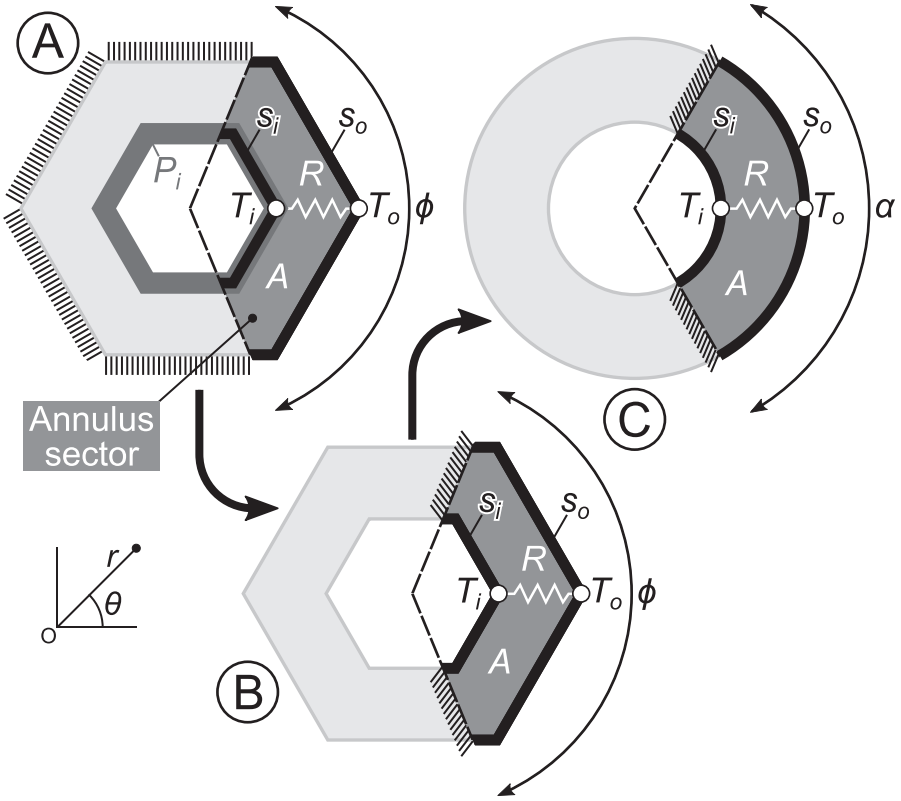

Fig. 3. Two-rule, equivalent concentric circular annulus model extended to consider a sector. "A" shows an arbitrary annulus subject to an isothermal boundary condition of an arbitrary portion, or sector, of its outer perimeter. The sector's outer boundary length, which is subject to an isothermal boundary condition of T_o, is denoted by s_o. The remaining outer perimeter is insulated (hatched lines); an arbitrary annulus sector of area A is now defined, distinguished from the entire annulus by the dark shaded region."A" to "B", the inner perimeter of the entire annulus, P_i, is also subject to an isothermal boundary condition of an arbitrary portion; however, the present model nullifies temperature gradients normal to the sector's angular extents (dashed lines). The model uses a portion of the inner perimeter, or the sector's inner boundary length, s_i, $s_i \leq P_i$, which is subject to an isothermal boundary condition of T_i, to calculate the shape factor. "B" to "C", the equivalent annulus sector is applied.

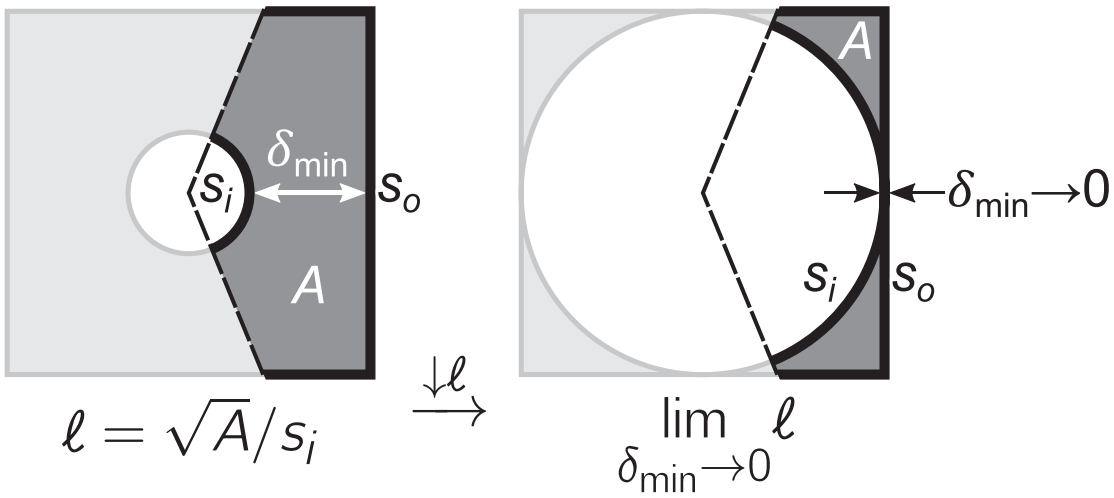

Fig. 4. Nonuniform wall thickness and thermal short-circuiting.

tors presented in this study. It is important to note that the equivalent sector angle is not affected by the blending, the nondimensional characteristic length scale, ℓ, appears in its expression as only an algebraic simplification. For equivalent sector angles above 2π, the sector is likened to an entire annulus and the modified two-rule method is used, Eq. (5).

For annulus sectors with uniform wall thickness, the present model, in Eq. (12), provides the shape factor of concentric annulus sectors as a function of two nondimensional parameters, the sector's nondimensional characteristic length scale, ℓ, and boundary length ratio, s_o/s_i. For nonuniform wall thickness, Eq. (13) uses a blending approach but still provides the shape factor as a function of only two nondimensional parameters, the sector's now-modified nondimensional characteristic length scale, ℓ^*, and boundary length ratio, s_o/s_i. Eqs. (12) and (13) provide simple, unified, and closed-form analytical solutions for the shape factor of arbitrarily-shaped concentric annulus sectors.

3. Results and discussion

To extensively validate the present model, sectors of parametrically-defined annuli with uniform and nonuniform wall thickness are numerically modeled using finite element modeling. Although the validated annuli represent simple geometries, their sectors do not. This validation considers well over a thousand distinct annulus sectors using well-defined parametric analysis. The consideration, and subsequent validation, of such a significant number of sectors affirms the present model's applicability to *arbitrary* geometry.

For this validation, the sector's inner isothermal boundary, is considered to span the entire inner perimeter (i.e., $s_i = P_i$). This tests the present model's assumption of insulated angular extent lines ("A" to "B" in Fig. 3). This setup is representative of conduction-limited applications, where the conduction thermal resistance far outweighs the convective (this is typical of most of the devices of interest to this modeling, such as those illustrated in Fig. 1).

Given that there is no available experimental data in the open literature to validate the present model, the parametrically-defined annulus sectors are modeled using finite element modeling (FEM) with the COMSOL Multiphysics software package v5.6 [13]. Two-dimensional, steady-state heat conduction is calculated using Laplace's equation:

$$\nabla^2 T = 0 \tag{14}$$

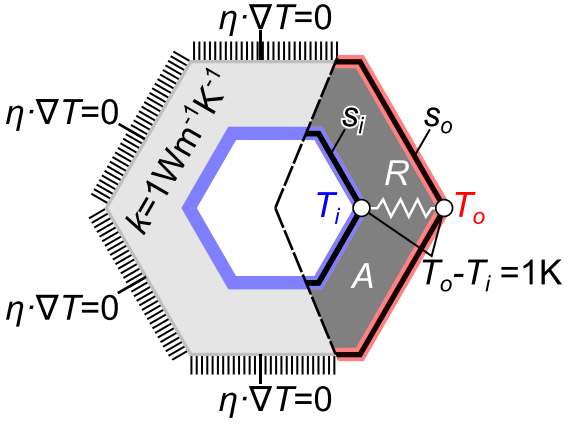

Fig. 5. Boundary conditions used in the finite element modeling. η is the unit normal vector. The temperature difference, $T_o - T_i$, and thermal conductivity, k, were chosen as 1K and $1\mathrm{Wm^{-1}K^{-1}}$, respectively.

with a relative tolerance of 0.001 used to determine numerical convergence [13]. Mixed boundary conditions were used in this study (Dirichlet and Neumann). As shown for an exemplar annulus sector in Fig. 5, Dirichlet conditions are imposed for the isothermal boundaries (i.e., T_i and T_o that span s_i and s_o, respectively). Neumann conditions are imposed for the out-of-sector, remaining outer boundary. This Neumann condition is insulative and expressed as:

$$\eta \cdot \nabla T = 0 \tag{15}$$

where η is the unit normal vector to the boundary.

Using Fourier's law, numerical data is integrated along the sector's outer isothermal boundary, s_o, to calculate the shape factor:

$$S = \frac{1}{kR} = \frac{\int_0^{s_o} \eta \cdot \nabla T ds}{(T_i - T_o)} \tag{16}$$

where η is the unit normal vector to the outer isothermal boundary, s_o. To simplify the calculation, the thermal conductivity, k, and temperature difference, $T_o - T_i$, were set to $1\mathrm{Wm^{-1}K^{-1}}$ and 1K, respectively, in the finite element modeling.

Mesh dependency studies were performed for all of the investigated annulus sectors. Given the specified boundary conditions, it was necessary to mesh entire annuli. As previously discussed, annulus sectors were defined by the applied boundary conditions

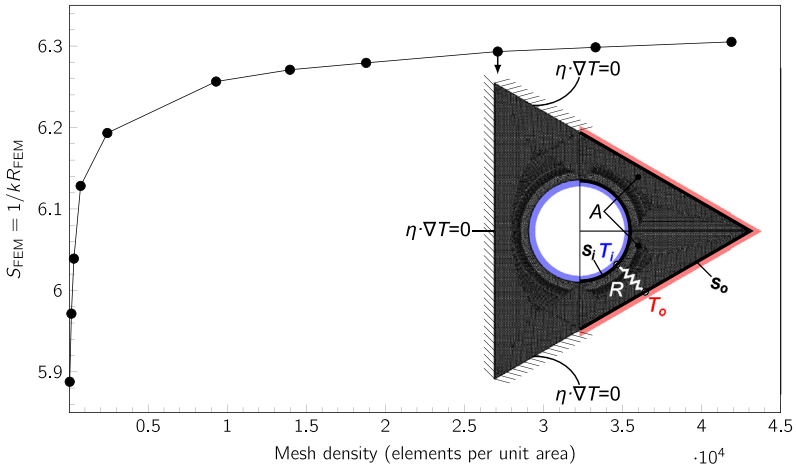

Fig. 6. Mesh dependence study. An annulus sector with highly nonuniform wall thickness was chosen for the illustrated exemplar given its entire annulus' larger relative differences from experimental data in the literature [9]. A minimum mesh density of about 25 000 elements per unit area was found to be sufficient for most of the investigated annulus sectors. Typically, the shape factor changed by less than 0.1% at this mesh density. FEM: finite element modeling.

(Fig. 3). A free triangular mesh was used for all of the investigated annuli.

As shown in Fig. 6, an exemplar mesh dependency study is shown for an annulus sector of highly nonuniform wall thickness. An annulus sector with highly nonuniform wall thickness was chosen for the illustrated exemplar given its entire annulus' larger relative differences from experimental data in the literature [9]. A minimum mesh density of about 25 000 elements per unit area was found to be sufficient for most of the investigated annulus sectors. Typically, the shape factor changed by less than 0.1% at this mesh density.

3.1. Uniform wall thickness

The model is validated for offset parametrically-identical boundaries, with the offset defined by a uniform wall thickness. The hyperellipse and regular polygon were chosen to define the boundaries parametrically, providing an exhaustive geometric analysis.

3.1.1. Hyperellipse

The hyperellipse, or LamĘ curve, is written in radial coordinates as follows [14,15]:

$$r(\theta) = a\left(|\cos\theta|^n + \epsilon^{-n}|\sin\theta|^n\right)^{-1/n} \tag{17}$$

where ϵ is the aspect ratio (ratio of the side lengths, non-unity aspect ratio geometries clarify this definition, shown in Fig. 9), n is the exponent parameter and a is the characteristic dimension. As shown in Fig. 7, changing the exponent parameter yields a variety of boundaries. For geometries with offset hyperellipse boundaries, the annulus is described as follows:

$$\begin{aligned} r_o(\theta) &= a\left(|\cos\theta|^n + \epsilon^{-n}|\sin\theta|^n\right)^{-1/n} \\ r_i(\theta) &= a\left\{[1-(\delta_0/a)]^{-n}|\cos\theta|^n + [\epsilon-(\delta_0/a)]^{-n}|\sin\theta|^n\right\}^{-1/n}, \quad n \geq 1 \end{aligned} \tag{18}$$

where r_o, r_i, and δ_0 are the outer and inner radial coordinates and the offset (wall thickness), respectively. As shown in Fig. 7, the wall thickness for a hyperelliptical annulus is defined as the thickness along the characteristic axes.

The parameters required to calculate the shape factor using the present model, Eq. (12), do not have closed-form solutions but can simply be calculated as follows:

$$\begin{aligned} \ell = \sqrt{A}/s_i &= \frac{\sqrt{\int_0^{\phi/2}\left(r_o^2 - r_i^2\right)d\theta}}{2\int_0^{\phi/2}\left[\sqrt{(dr_i/d\theta)^2 + r_i^2}\right]d\theta} \\ s_o/s_i &= \frac{\int_0^{\phi/2}\left[\sqrt{(dr_o/d\theta)^2 + r_o^2}\right]d\theta}{\int_0^{\phi/2}\left[\sqrt{(dr_i/d\theta)^2 + r_i^2}\right]d\theta} \end{aligned} \tag{19}$$

where ϕ, ℓ, and s_o/s_i are the sector angle, nondimensional characteristic length scale, and boundary length ratio, respectively. Using Eqs. (18) and (19) in the present model, the nondimensional inputs for the shape factor, ℓ and s_o/s_i, can be expressed as a function of the sector angle, ϕ, the exponent parameter, n, and two ratios, thickness ratio, δ_0/a, and aspect ratio, ϵ.

The present model is plotted against the nondimensional characteristic length scale, ℓ, and compared to the results from finite element modeling (FEM) in Figs. 8 and 9. The results from finite element modeling were obtained by sweeping through sector angles for chosen thickness and aspect ratios. The minimum investigated sector angles are listed in Table A.1 in Appendix A. The relationship between the sector's geometric parameters and nondimensional characteristic length scale is shown in Eqs. (18) and (19). For a hyperelliptical annulus with a given aspect ratio and exponent parameter, the nondimensional characteristic length scale increases with increasing thickness ratio and decreases with increasing sector angle (i.e., thicker, smaller angle sectors have higher nondimensional characteristic length scales). For example, the exact relationship for a circular annulus sector, $n = 2$ and $\epsilon = 1$, can be written as follows:

$$\ell_{n=2,\epsilon=1} = \left(\sqrt{A}/s_i\right)_{n=2,\epsilon=1} = \frac{1}{\sqrt{2\phi}}\frac{\sqrt{2(\delta_0/a) - (\delta_0/a)^2}}{1-(\delta_0/a)} \tag{20}$$

where ϕ and δ_0/a are the sector angle and thickness ratio, respectively.

Hyperelliptical sectors with an aspect ratio of one have a boundary length ratio that is only a function of the thickness ratio, $(s_o/s_i)_{\epsilon=1} = 1/[1-(\delta_0/a)]$, and thus, a single curve for each thickness ratio is shown in Fig. 8. For non-unity aspect ratios, the boundary length ratio is also a function of the sector angle, the aspect ratio, and the exponent param-

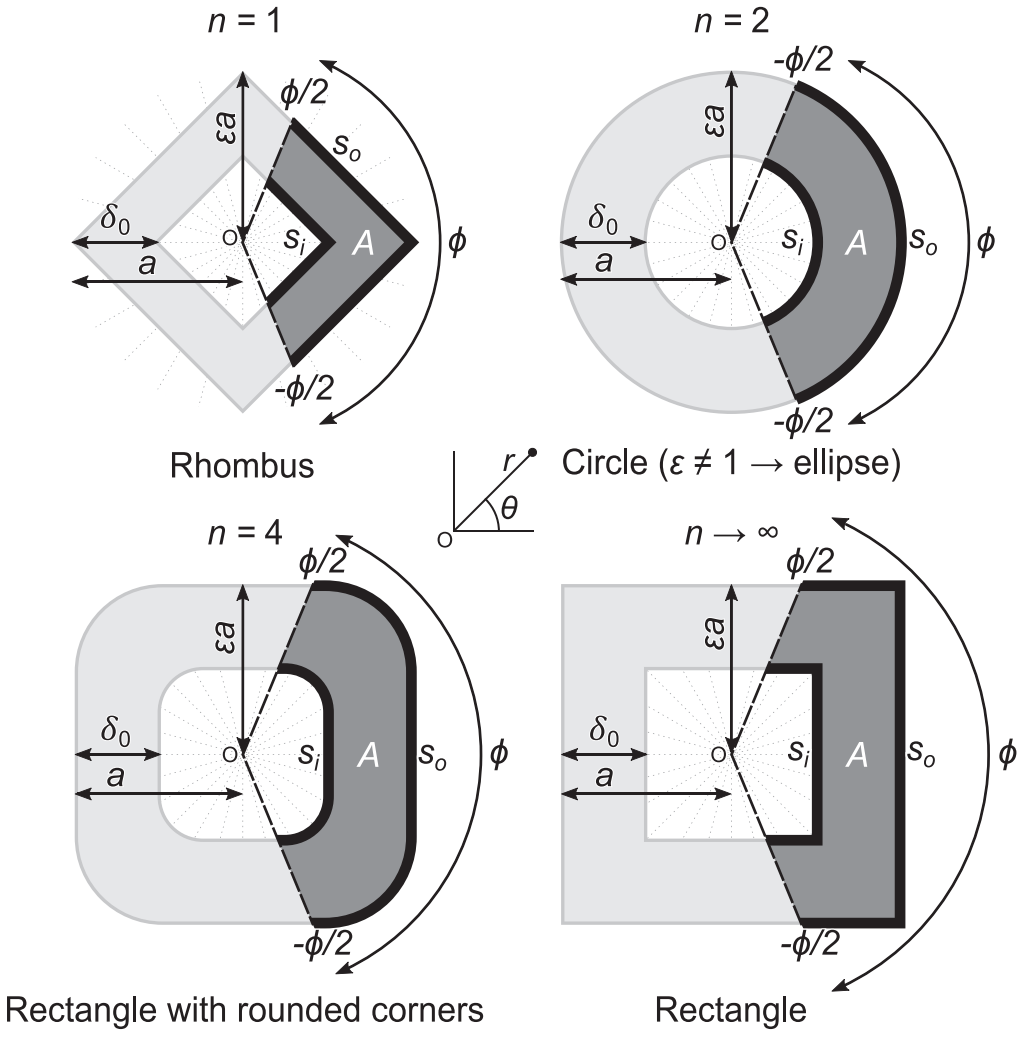

Fig. 7. Hyperelliptical annulus sectors. A ratio of the side lengths, or aspect ratio, of unity is shown, $\epsilon = 1$.

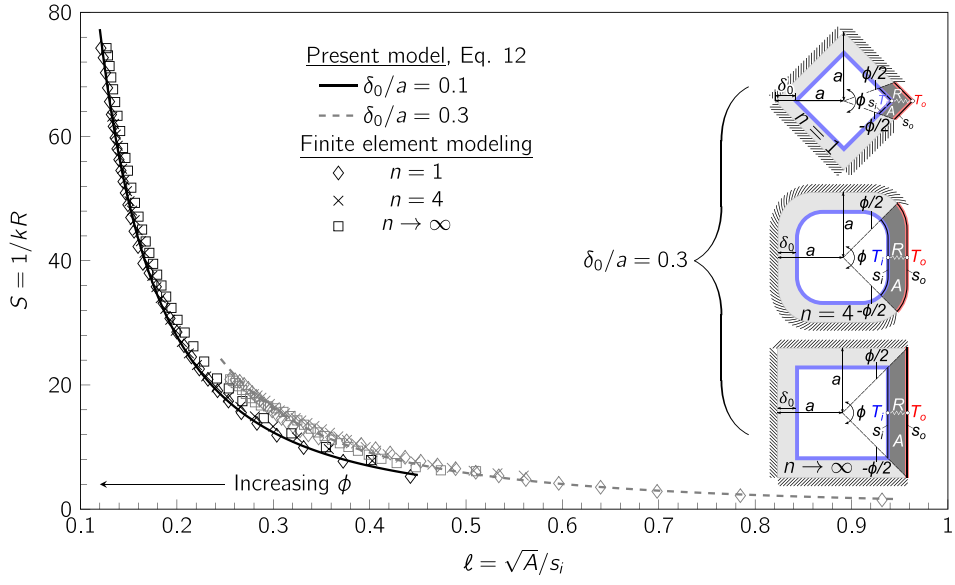

Fig. 8. Model validation for hyperelliptical sectors, $\epsilon = 1$.

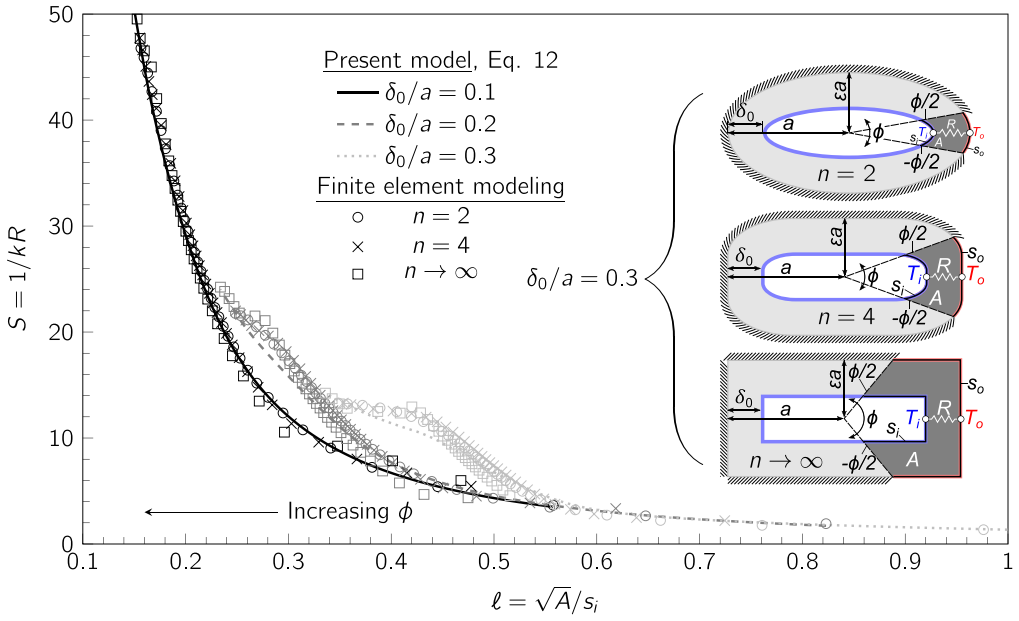

Fig. 9. Model validation for hyperelliptical sectors, $\epsilon = 1/2$.

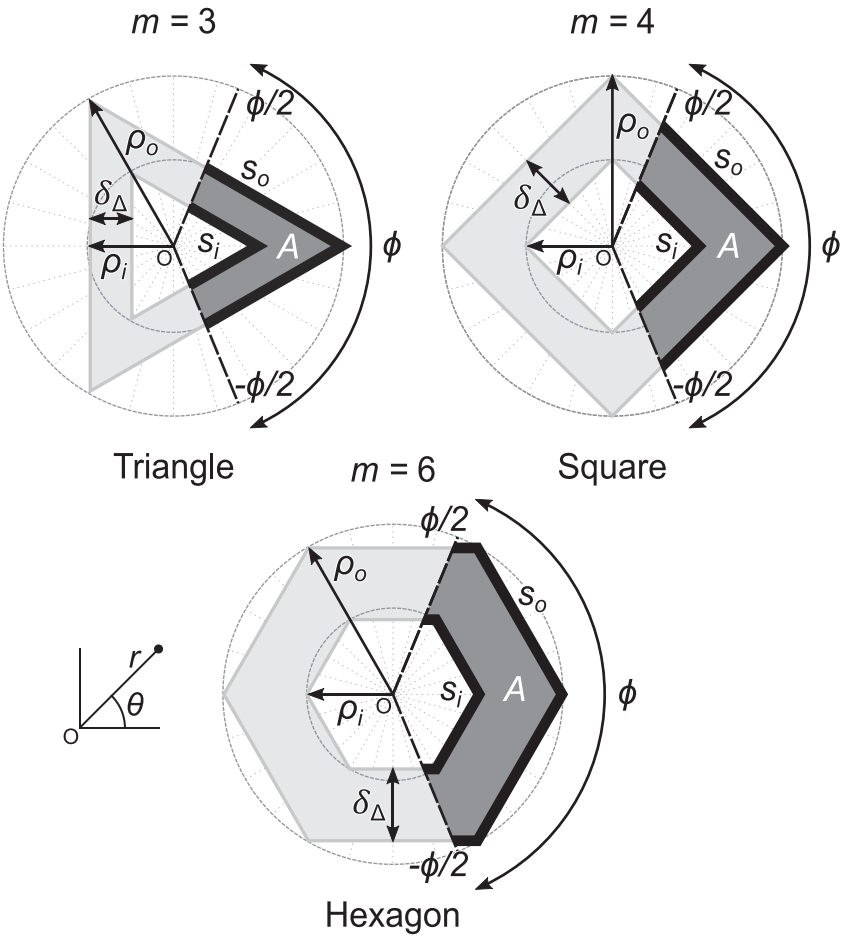

Fig. 10. Regular polygonal annulus sectors.

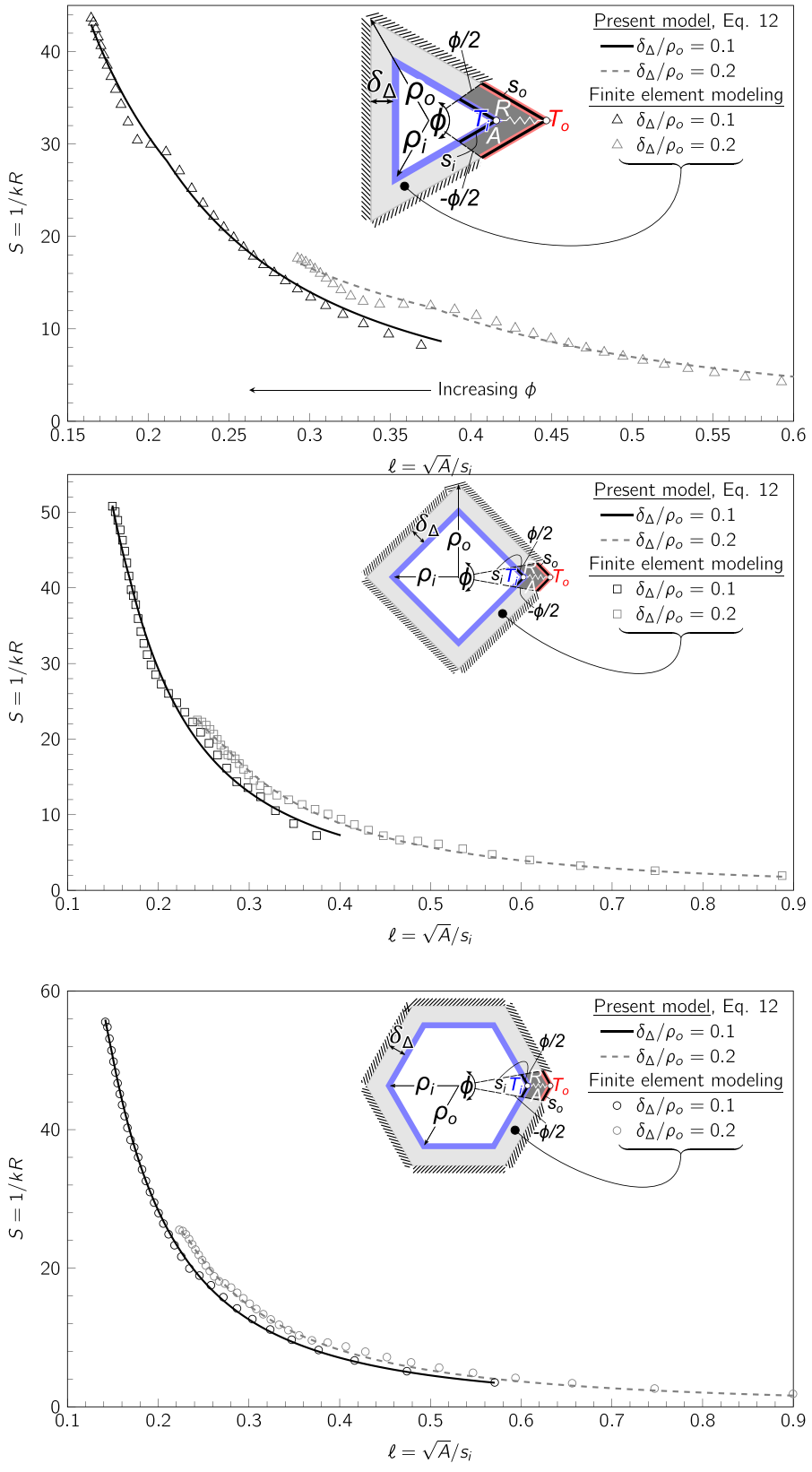

Fig. 11. Model validation for regular polygonal annulus sectors.

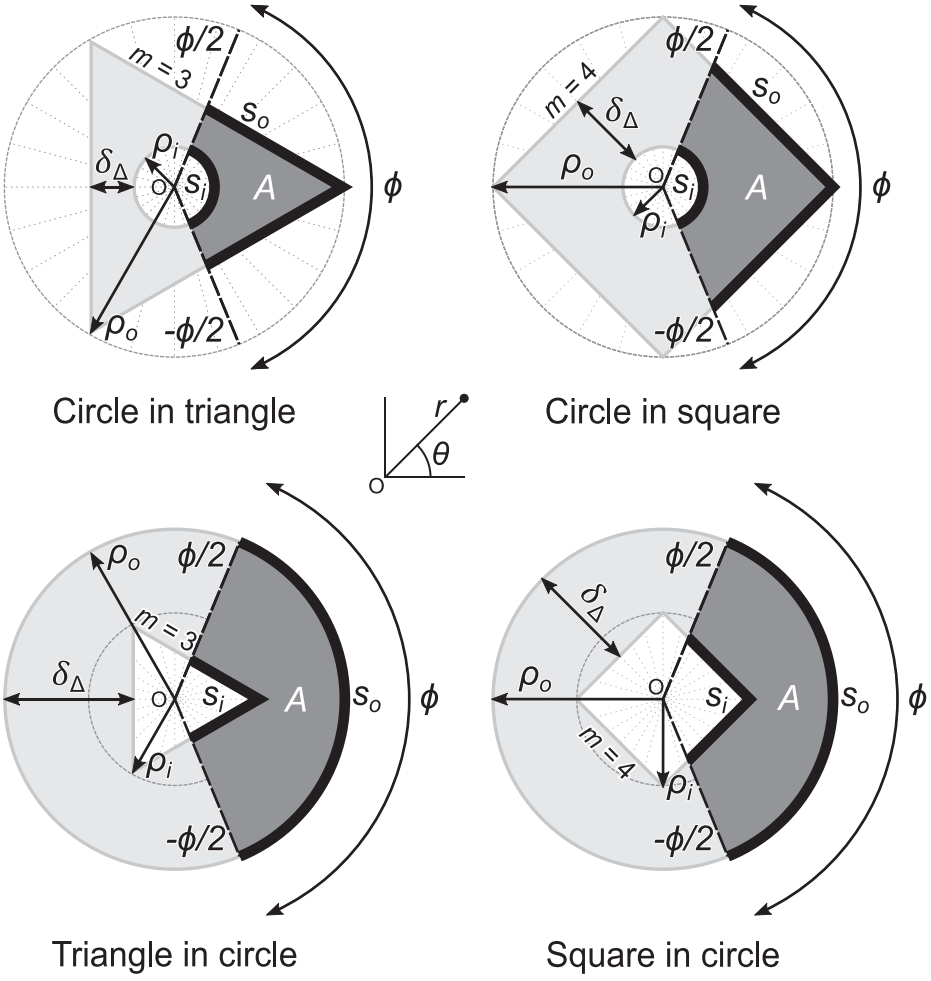

Fig. 12. Annulus sectors with nonuniform wall thickness.

eter. However, for the chosen hyperelliptical annulus sectors, these differences are slight and not graphically apparent, and thus, a single curve for each thickness ratio is also shown in Fig. 9.

The present model showed good agreement with results from finite element modeling and accurately captured trends for varying exponent parameters, aspect ratios, sector angles, and wall thicknesses. As shown in Table A.1 in Appendix A, the root-mean-square (rms) and maximum differences between the results from the present model and finite element modeling was less than 10 and 20%, respectively, for all investigated sectors. As shown in Figs. 8 and 9, sectors with larger thickness ratios and smaller sector angles typically had more considerable relative differences owing to the nature of the underlying two-rule method and the stated assumptions. Thick, small-angle sectors intuitively pushed the limits of the present model, exhibiting isotherms that were more consistent with thermal spreading resistance modeling than equivalently radial, or parallel to the inner and outer boundaries (s_i and s_o). For most of the investigated hyperelliptical sectors, this limit was at a nondimensional length scale of about 0.55. To re-iterate, these results indicated that the key limitation of the present model is that it may be unreliable for thick, small-angle sectors with nondimensional length scales above 0.55. For the exemplar annulus in Eq. (20) and an exemplar sector angle of $\pi/2$, or a quarter annulus, this nondimensional length scale corresponds to a thickness ratio of about 0.3, consistent with the maximum investigated value in the validation.

Typically, the shape factor exponentially increases for a decreasing nondimensional characteristic length scale. As previously exemplified in Eq. (20), an increase in the sector angle or decrease in the wall thickness decreases the nondimensional characteristic length scale. In other words, as one would intuitively expect, the shape factor of an annulus sector is maximized by minimizing the wall thickness and maximizing the sector angle.

3.1.2. Regular polygon

The m-sided inscribed regular polygon is mathematically written in radial coordinates as follows:

$$r(\theta) = \frac{\rho \cos(\pi/m)}{\cos\{(2/m)\arcsin[\cos(m\theta/2)]\}}, \quad m = 3, 4, 5, \ldots \tag{21}$$

where m and ρ are the number of sides and circumradius, respectively. As shown in Fig. 10, changing the number of sides yields various polygons, including the equilateral triangle, square, and hexagon. For geometries with offset regular polygonal boundaries, the annulus is described as follows:

$$r_o(\theta) = \frac{\rho_o \cos(\pi/m)}{\cos\{(2/m)\arcsin[\cos(m\theta/2)]\}}, \quad m = 3, 4, 5, \ldots$$

$$r_i(\theta) = \frac{\rho_o\{1-[(\delta_\Delta/\rho_o)/\cos(\pi/m)]\}\cos(\pi/m)}{\cos\{(2/m)\arcsin[\cos(m\theta/2)]\}}, \quad m = 3, 4, 5, \ldots \tag{22}$$

where ρ_o, r_o, r_i and δ_Δ are the outer circumradius, outer and inner radial coordinates, and apothem-to-apothem wall thickness, respectively.

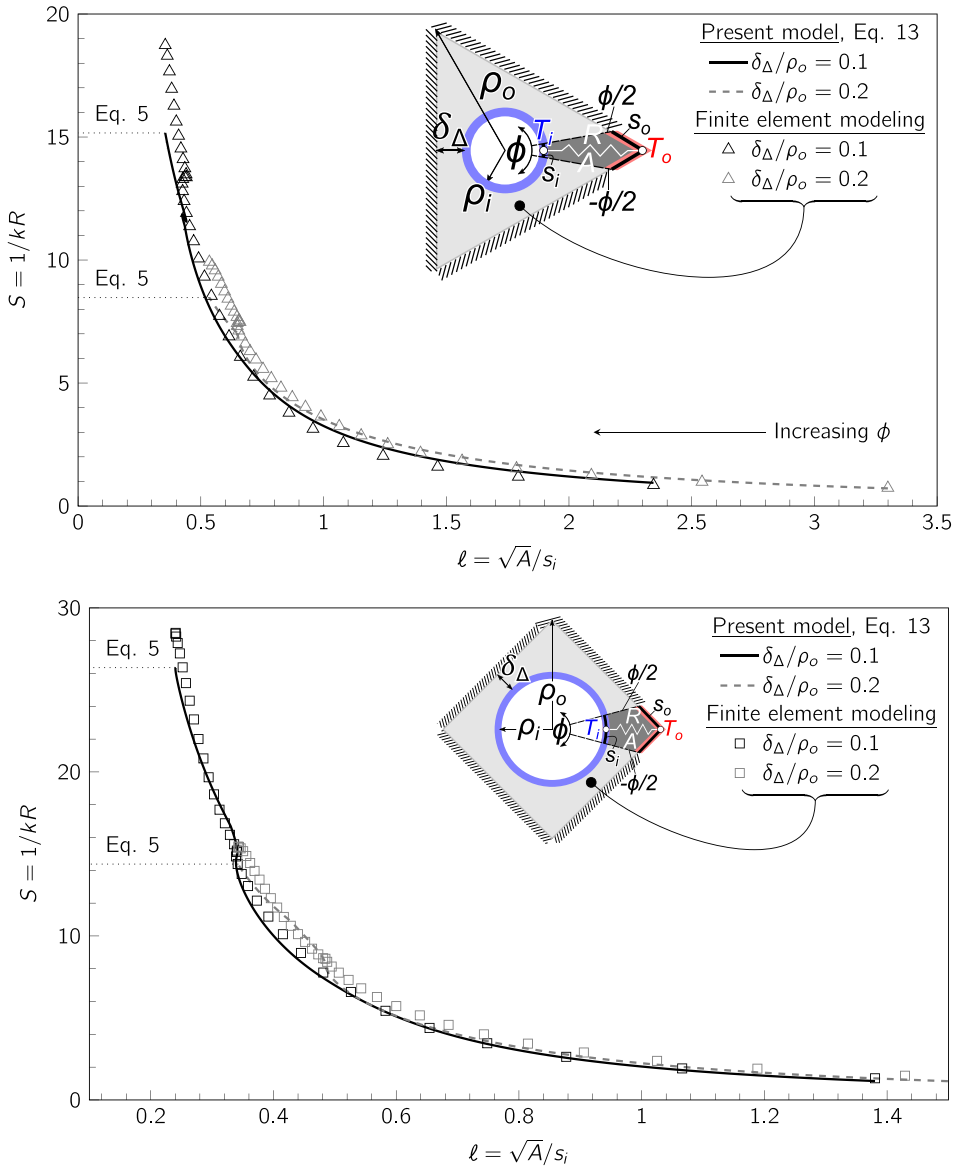

Fig. 13. Model validation for nonuniform wall thickness.

Like the hyperelliptical sector, the parameters required to calculate the shape factor using the present model, Eq. (12), do not have closed-form solutions and must be calculated with Eq. (19). Using Eqs. (19) and (22) in the present model, the nondimensional inputs for the shape factor, ℓ and s_o/s_i, can be expressed as a function of the sector angle, ϕ, the number of sides, m, and the thickness ratio, δ_Δ/ρ_o.

The present model is plotted against the nondimensional characteristic length scale, ℓ, and compared to the results from finite element modeling (FEM) in Fig. 11. The results from finite element modeling were obtained by sweeping through sector angles for chosen thickness ratios. The minimum investigated sector angles are listed in Table A.2 in Appendix A. The relationship between the sector's geometric parameters and nondimensional characteristic length scale was previously discussed in Section 3.1.1.

Polygonal annulus sectors have a boundary length ratio that is a function of all of the geometric parameters: sector angle, number of sides, and thickness ratio. Therefore, as opposed to the hyperelliptical annulus sector plots, Figs. 8 and 9, results from the present model for polygonal annulus sectors were distinct and could not be collapsed to similar curves.

The present model showed good agreement and accurately captured trends for varying numbers of sides, sector angles, and wall thicknesses. As shown in Table A.2 in Appendix A, the root-mean-square (rms) and maximum differences between the results from the present model and finite element modeling was less than 6 and 16%, respectively, for all investigated sectors. As shown in Fig. 11 and discussed in Section 3.1.1, sectors with larger thickness ratios and smaller sector angles typically had more considerable relative differences owing to the nature of the underlying two-rule method and the stated assumptions. Consistent with observations for hyperelliptical annulus sectors, the limit for reliable agreement was at a nondimensional length scale of about 0.55.

3.2. Nonuniform wall thickness

The model also considers sectors with highly nonuniform wall thickness, defined by distinct boundaries. As shown in Fig. 12, this

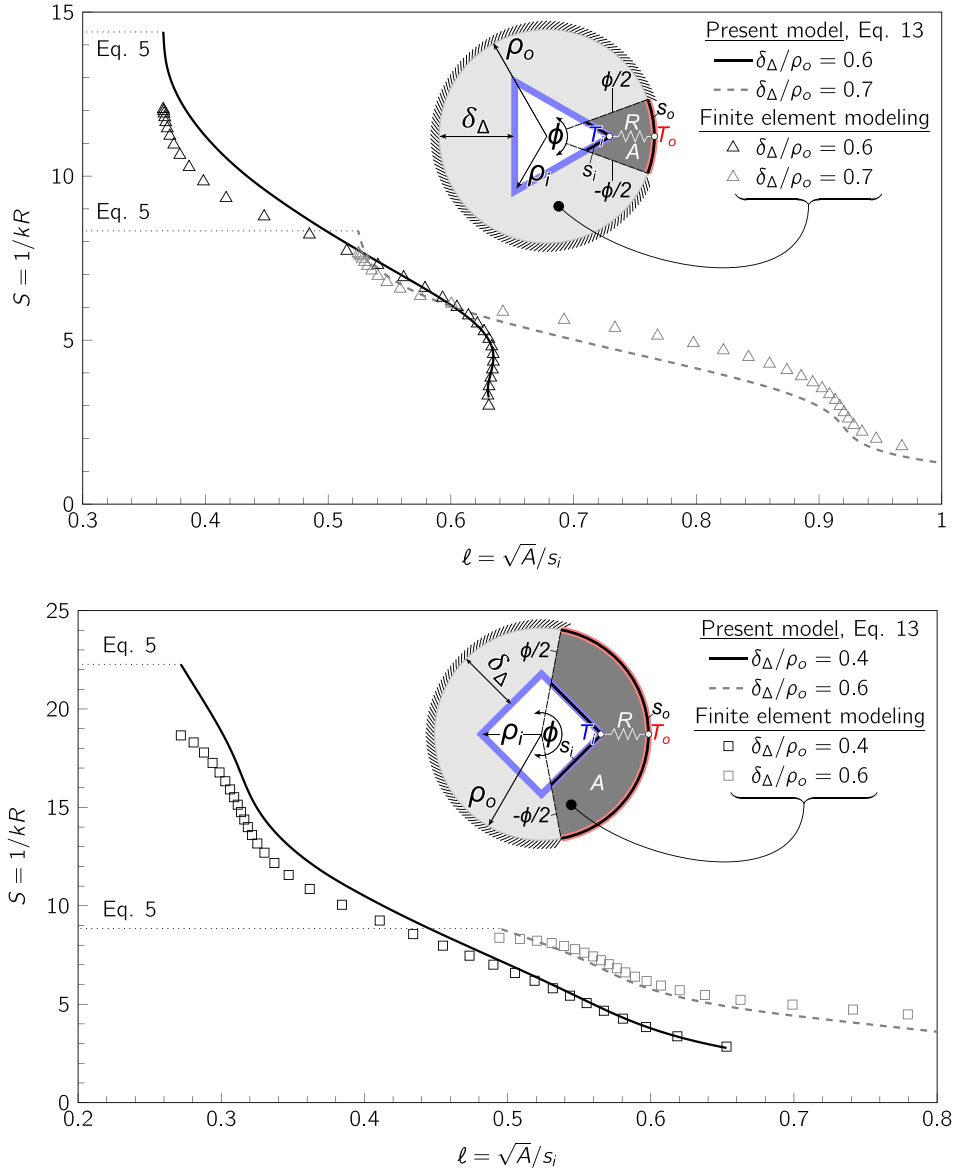

Fig. 13. Continued

analysis considers varying-sided regular polygons outside and inside a circle. Using Eq. (22), the boundaries are written in radial coordinates as follows:

$$r_o(\theta) = \frac{\rho_o \cos(\pi/m)}{\cos\{(2/m)\arcsin[\cos(m\theta/2)]\}}, \quad m = 3, 4, 5, \ldots,$$
$$r_i(\theta) = \rho_o[1 - (\delta_\Delta/\rho_o)] \tag{23}$$

for the circle in polygon and:

$$r_o(\theta) = \rho_o$$
$$r_i(\theta) = \frac{\rho_o\{1 - [(\delta_\Delta/\rho_o)/\cos(\pi/m)]\}\cos(\pi/m)}{\cos\{(2/m)\arcsin[\cos(m\theta/2)]\}}, \quad m = 3, 4, 5, \ldots, \tag{24}$$

for the polygon in circle, where ρ_o, m, δ_Δ, r_o and r_i are the outer circumradius, number of polygon sides, apothem wall thickness, and outer and inner radial coordinates, respectively.

The parameters required to calculate the shape factor using the present model, Eq. (13), do not have closed-form solutions but can be calculated with Eq. (19). Using Eqs. (19) and (23) or (19) and (24) in the present model, the nondimensional inputs for the shape factors of circle in polygon or polygon in circle sectors, ℓ and s_o/s_i, can be expressed as a function of the sector angle, ϕ, the number of sides, m, and the thickness ratio, δ_Δ/ρ_o.

The present model is plotted against the nondimensional characteristic length scale, ℓ, and compared to results from finite element modeling (FEM) in Fig. 13. Results from finite element modeling were obtained by sweeping through sector angles for chosen thickness ratios. The minimum investigated sector angles are listed in Table A.3 in Appendix A. As previously mentioned in the stated assumptions, isotherms are assumed to be equivalently radial (i.e., parallel to the inner and outer boundaries, s_i and s_o) in the present model. Thus, to avoid sectors that may be better modeled with a thermal spreading resistance, only larger sector angles were considered to validate the thicker circular cylinder with a square hole. These sector angles were chosen to keep the investigated nondimensional characteristic length scale range comparable to the thicker circular cylinder with a triangular hole. The relationship between the sector's geometric parameters and nondimensional characteristic length scale was previously discussed in Section 3.1.1.

The present model showed good agreement and accurately captured trends for varying numbers of sides, sector angles, and wall thicknesses. As shown in Table A.3 in Appendix A, the root-mean-square (rms) and maximum differences between results from the present model and finite element modeling was less than 13 and 20%, respectively, for all investigated sectors. There was no definitive trend concerning the relative difference and the nondimensional characteristic length scale, owing to the asymptotic blending modification to the underlying two-rule method. However, as shown in Fig. 13, the present model outperformed the underlying two-rule method, Eq. (5), compensating for the significant relative difference in the shape factor of the entire annulus.

A walk-through of simple example problems is provided in the supplementary material. This walk-through highlights the simplicity of the present model, where a potentially complicated problem in Laplace's equation (Eq. (14)) with mixed boundary conditions is reduced to a geometry problem involving the calculation of a few dimensions. This simplification allows for computationally-inexpensive parametric analysis (e.g., the same type of analysis used in the subsequent validation) and optimization for problems involving the calculation of conduction thermal resistance in an annulus sector (as previously mentioned, many problems do, see Fig. 1). These analyses involve many iterations that re-calculate the output, in this case, the shape factor (or thermal resistance). Numerically, these analyses would involve many re-evaluations of Laplace's equation subject to mixed boundary conditions, thus, scaling the already significant computational performance gap between the present model and numerical models. Similar reasoning could be applied to the advantageous use of the present model in lumped parameter modeling involving many different complicated geometries and transport mechanisms (e.g., convective heat [16] and mass [17]). In short, the present model's simplicity, ease of use, and computational efficiency are its key advantages over more intensive numerical modeling.

4. Summary and conclusions

A new analytical model was developed to predict the conduction shape factor for the annulus sector formed between arbitrarily shaped isothermal inner and outer boundaries. In summary, the present model was:

- derived from the equivalent concentric circular annulus sector, as an extension of the equivalent concentric circular annulus [8,9],
- extended to consider annulus sectors with nonuniform wall thickness, and,
- extensively validated with finite element modeling results for more than a thousand parametrically-defined annulus sectors with uniform and nonuniform wall thickness, capturing most of the results from finite element modeling within a relative difference of 10%, and all results within a relative difference of 20%.

Declaration of Competing Interest

The authors declare that they have no known competing financial interests or personal relationships that could have appeared to influence the work reported in this paper.

CRediT authorship contribution statement

Callum Chhokar: Conceptualization, Methodology, Investigation, Validation, Writing – original draft. **G. Bamorovat Abadi:** Conceptualization, Writing – review & editing. **Majid Bahrami:** Supervision, Writing – review & editing.

Acknowledgements

The authors gratefully acknowledge the financial support of the Natural Sciences and Engineering Research Council of Canada (NSERC) under the College-University Idea to Innovation Grant No. 470927-14 and Innovation BC under the Ignite program.

Appendix A. The minimum investigated sector angles and agreement with finite element modeling data

Table A1
The minimum investigated sector angles and percentage differences (minimum, root-mean-square, and maximum) between the present model and the results from finite element modeling for hyperelliptical annulus sectors.

$\epsilon = 1$			
		δ_0/a	
$\phi_{\min}$ min/rms/max	0.1	0.2	0.3
$n =$	20°	20°	20°
1	0/2/8%	0/5/17%	0/6/13%
$n =$	40°	70°	90°
4	1/4/12%	1/5/14%	1/7/14%
$n \rightarrow$	40°	80°	90°
∞	0/4/13%	0/4/15%	0/4/8%
	$\epsilon = 1/2$		
		δ_0/a	
$\phi_{\min}$ min/rms/max	0.1	0.2	0.3
$n =$	20°	20°	20°
2	0/3/4%	0/6/10%	1/10/15%
$n =$	20°	40°	40°
4	0/5/17%	0/6/10%	0/10/15%
$n \rightarrow$	30°	50°	90°
∞	0/5/15%	0/8/25%	0/9/20%

Table A2
The minimum investigated sector angles and percentage differences (minimum, root-mean-square, and maximum) between the present model and the results from finite element modeling for regular polygonal annulus sectors.

	δ_Δ/ρ_o	
$\phi_{\min}$ min/rms/max	0.1	0.2
$m =$	50°	70°
3	0/4/13%	0/6/16%
$m =$	50°	20°
4	0/5/15%	0/5/11%
$m =$	20°	20°
6	0/2/3%	0/6/13%

Table A3
The minimum investigated sector angles and percentage differences (minimum, root-mean-square, and maximum) between the present model and results from finite element modeling for the nonuniform wall thickness sectors.

Circle in polygon		
	δ_Δ/ρ_o	
$\phi_{\min}$ min/rms/max	0.1	0.2
$m =$	20°	20°
3	1/13/19%	0/9/15%
$m =$	20°	30°
4	1/6/13%	0/8/16%
	Polygon in circle	
		δ_Δ/ρ_o
$\phi_{\min}$ min/rms/max	0.4	0.6	0.7
$m =$	-	50°	40°
3		0/11/20%	1/13/17%
$m =$	30°	160°	-
4	0/11/19%	1/7/16%	

Supplementary material

Supplementary material associated with this article can be found, in the online version, at doi:10.1016/j.ijheatmasstransfer.2022.123304

References

[1] L.M. Simeza, M.M. Yovanovich, Shape factors for hollow prismatic cylinders bounded by isothermal inner circles and outer regular polygons, Int. J. Heat Mass Transf. 30 (4) (1987) 812–816, doi:10.1016/0017-9310(87)90213-4.

[2] F.P. Incropera, D.P. DeWitt, T.L. Bergman, A.S. Lavine, Principles of Heat and Mass Transfer, volume 7, John Wiley & Sons, 2013.

[3] K.T. Lin, S.C. Wong, Performance degradation of flattened heat pipes, Appl. Therm. Eng. 50 (1) (2013) 46–54, doi:10.1016/j.applthermaleng.2012.06.001.

[4] Mouser Electronics®, Advanced thermal solutions high performance round & flat heat pipes. https://www.mouser.com/new/advanced-thermal-solutions/ats-heat-pipes/.

[5] M.B. Shafii, S. Arabnejad, Y. Saboohi, H. Jamshidi, Experimental investigation of pulsating heat pipes and a proposed correlation, Heat Transf. Eng. 31 (10) (2010), doi:10.1080/01457630903547636.

[6] M. Winkler, D. Rapp, A. Mahlke, F. Zunftmeister, M. Vergez, E. Wischerhoff, J. Clade, K. Bartholomé, O. Schäfer-Welsen, Small-sized pulsating heat pipes/oscillating heat pipes with low thermal resistance and high heat transport capability, Energies 13 (7) (2020), doi:10.3390/en13071736.

[7] N. Tran, Y.J. Chang, J. Teng, R. Greif, A study on five different channel shapes using a novel scheme for meshing and a structure of a multi-nozzle microchannel heat sink, Int. J. Heat Mass Transf. 105 (2017) 429–442, doi:10.1016/j.ijheatmasstransfer.2016.09.076.

[8] P.M. Teertstra, M.M. Yovanovich, J.R. Culham, Analytical modeling of natural convection in horizontal annuli, in: Proceedings of the 43rd AIAA Aerospace Sciences Meeting and Exhibit - Meeting Papers, American Institute of Aeronautics and Astronautics, Reston, Virigina, 2005, pp. 3699–3708, doi:10.2514/6.2005-959.

[9] P.M. Teertstra, M.M. Yovanovich, J.R. Culham, Conduction shape factor models for hollow cylinders with nonuniform gap spacing, J. Thermophys Heat Transf. 23 (1) (2009) 28–32, doi:10.2514/1.35572.

[10] H.G. Elrod, Two simple theorems for establishing bounds on the total heat flow in steady-state heat-conduction problems with convective boundary conditions, J. Heat Transf. 96 (1) (1974) 65–70, doi:10.1115/1.3450142.

[11] A.V. Hassani, K.G. Hollands, G.D. Raithby, A close upper bound for the conduction shape factor of a uniform thickness, 2D layer, Int. J. Heat Mass Transf. 36 (12) (1993) 3155–3158, doi:10.1016/0017-9310(93)90044-7.

[12] K. Hirbodi, K. Jafarpur, A simple and accurate model for conduction shape factor of hollow cylinders, Int. J. Therm. Sci. 153 (October 2019) (2020) 106362, doi:10.1016/j.ijthermalsci.2020.106362.

[13] COMSOL AB, COMSOL Multiphysics® v. 5.6. https://www.comsol.com.

[14] J. Gielis, A generic geometric transformation that unifies a wide range of natural and abstract shapes, Am. J. Bot. 90 (3) (2003), doi:10.3732/ajb.90.3.333.

[15] N.T. Gridgeman, Lamé ovals, Math. Gazette 54 (387) (1970), doi:10.2307/3613154.

[16] Y.T. Tsui, B. Tremblay, On transient natural convection heat transfer in the annulus between concentric, horizontal cylinders with isothermal surfaces, Int. J. Heat Mass Transf. 27 (1) (1984), doi:10.1016/0017-9310(84)90242-4.

[17] M. Dejam, H. Hassanzadeh, The role of a porous wall on the solute dispersion in a concentric annulus, Phys. Fluids 33 (11) (2021), doi:10.1063/5.0070653.